Supplementary Figures

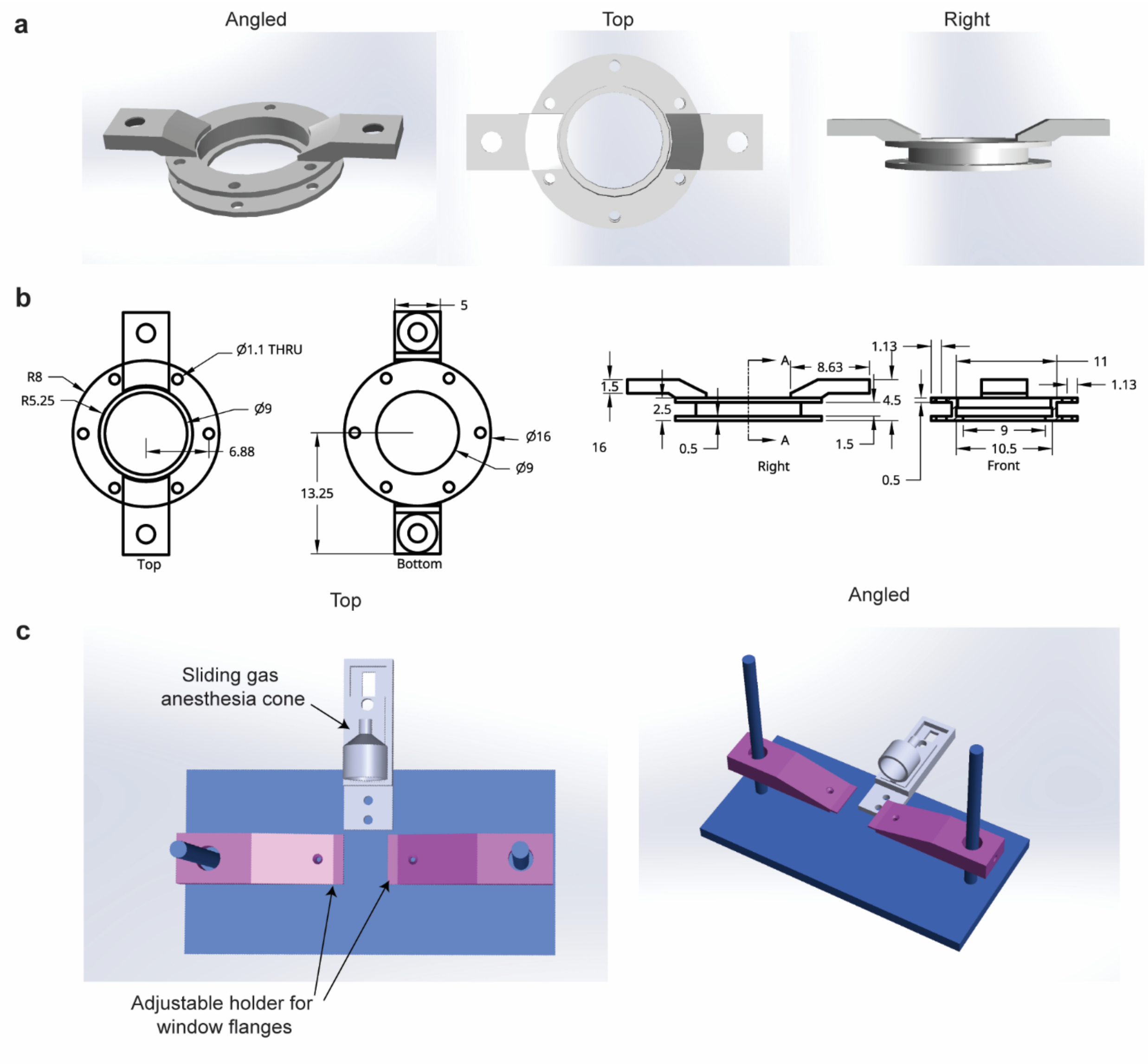

Figure S1| The design and fabrication of custom-made imaging window chamber and imaging stage. a, Angled, top, and right-side views of the 3-D printed imaging window. **b,** Dimensions of imaging window chamber (dimensions in mm) **c,** Top and angled view of imaging stage.

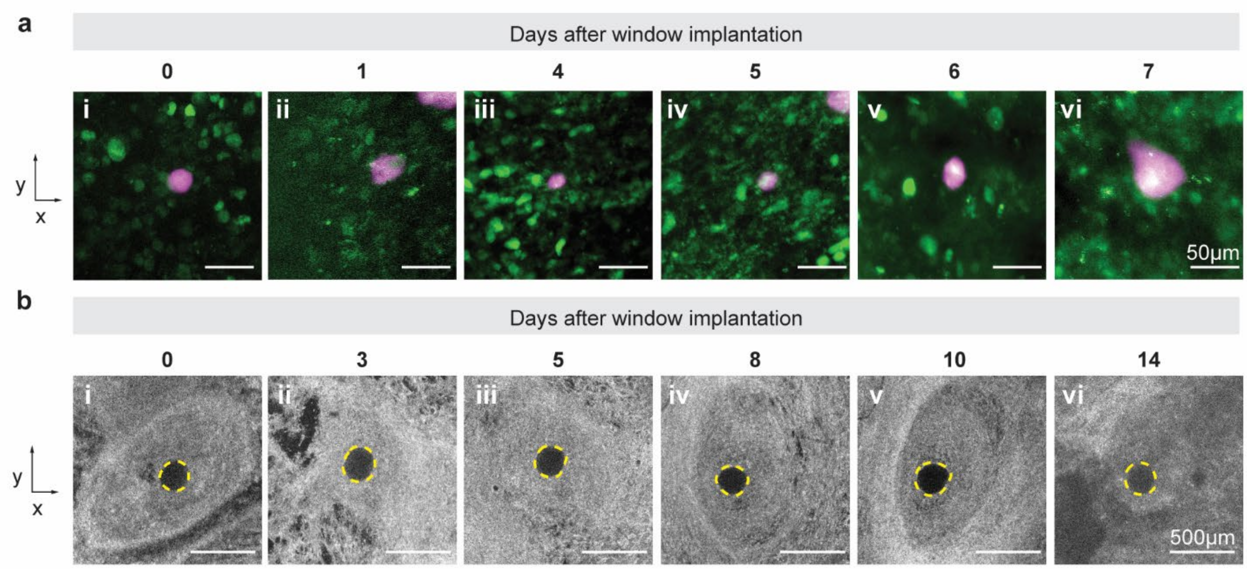

Figure S2| Longitudinal *in vivo* imaging of MCa-M3C-H2B-dendra2 tumors at the cellular and tissue scale. **a,** Cellular-scale beads were imaged up to 7 days via two-photon microscopy (cancer cells (green), PA beads (magenta)) and **b,** tissue-scale beads were tracked up to 14 days via optical coherence microscopy (PA bead (outlined in yellow)).

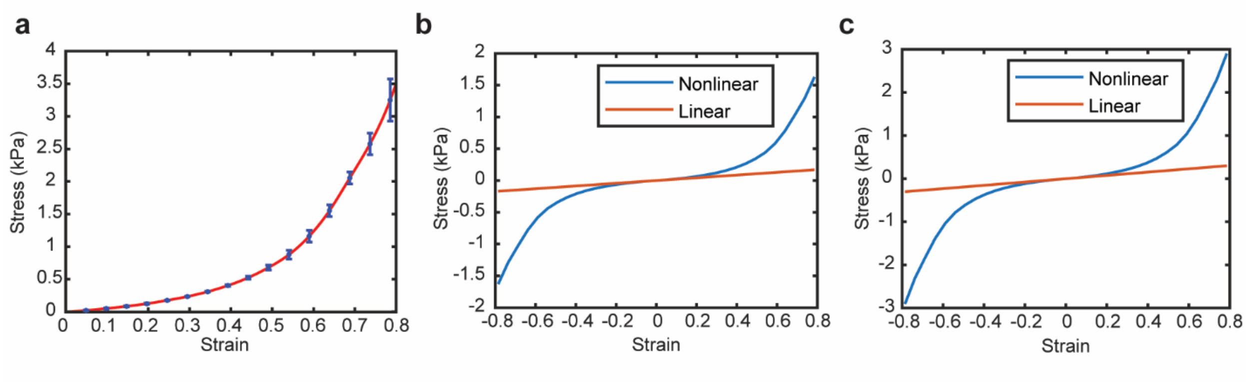

Figure S3| Nonlinear behavior of polyacrylamide gels. a, Axial compression curve of polyacrylamide gel. **b,** fitting nonlinear curve to cellular-scale bead Young's modulus of 215 Pa. **c,** fitting nonlinear curve to tissue scale bead Young's modulus of 383 Pa.

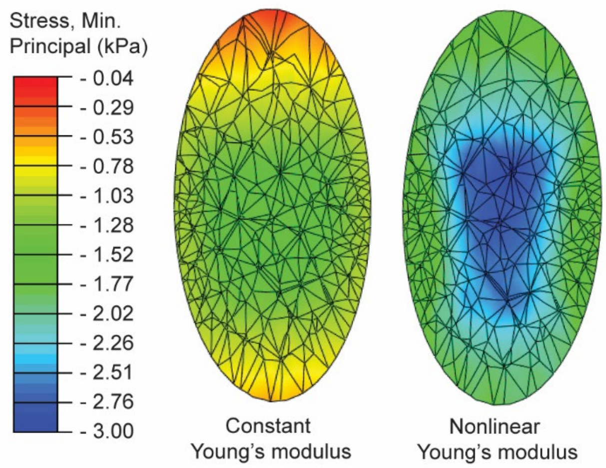

Figure S4| Comparison of constant Young's modulus (linear stress/strain) and nonlinear Young's modulus using hyperelastic FEM. Cross-section of tissue-scale FE model. The average of the maximum absolute principal stresses is 752 Pa when constant Young's modulus is used, compared to 1475 Pa when nonlinear Young's modulus is used.

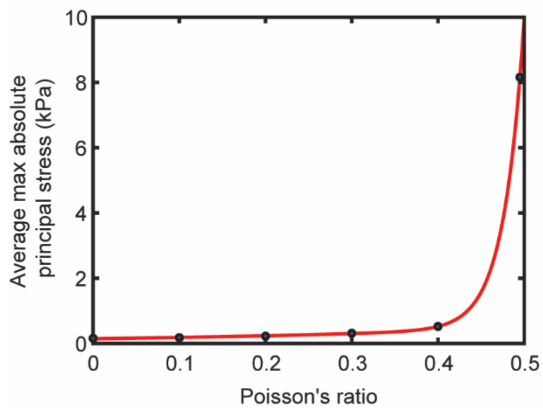

Figure S5| Parametric study of the effect of Poisson's ratio on FEM stress values. The Poisson's ratio was parametrically altered between 0 (ideal compressible material) and 0.5 (ideal incompressible material) in a finite-element model and resulted in exponentially increasing average max absolute principal stress values as Poisson's ratio approaches 0.5.

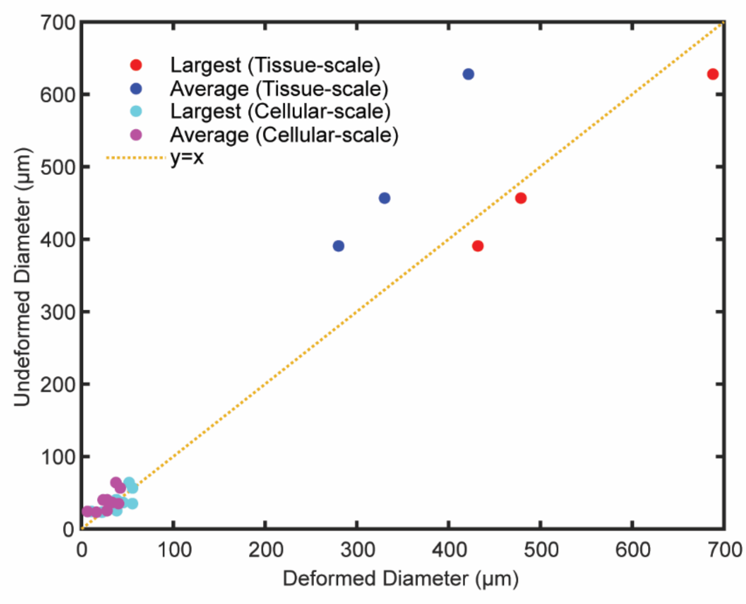

Figure S6| Original diameter selection for bead analysis. To determine the closest approximation for the undeformed diameter of beads, deformed beads in spheroids were relaxed via enzymatic dissociation of the spheroid with trypsin. The values for the undeformed diameter of each deformed bead was determined via enzymatic dissociation of the spheroid to relax the deformed beads. Assuming the undeformed diameter is the true original diameter, y=x is the ideal prediction line. The R^2 value is 0.692 when using the average deformed diameter as the original diameter compared to an R^2 value of 0.988 when using the largest deformed diameter as the original diameter. The largest diameter of the deformed bead is the closest estimate for the diameter of the undeformed bead. (n=7 cellular-scale beads, 3 tissue-scale beads)

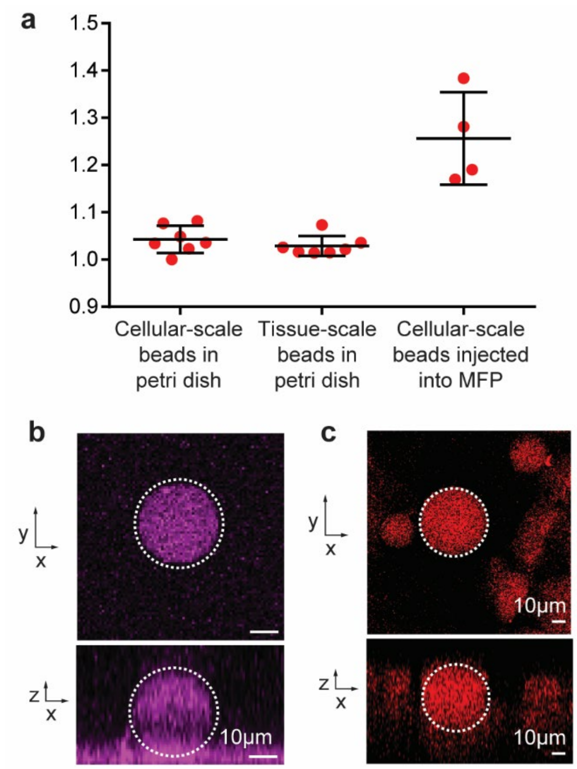

Figure S7| Injection through needle does not result in deformation in cellular- and tissue-scale beads. **a,** Measurement of bead aspect ratios after injecting through 25G (cellular scale) and 22G (tissue scale) needles into petri dish are close to 1 (mean ± STD, n=4-7 beads)**. b,** Bead after injecting through needle, XY and XZ views (bead (dotted white outline)). **c,** Bead after injecting into mammary fat pad of mouse without any tumor (bead (dotted white outline)). The lack of any distinct deformation demonstrates that the PA beads were not deformed prior to the development of the tumor.

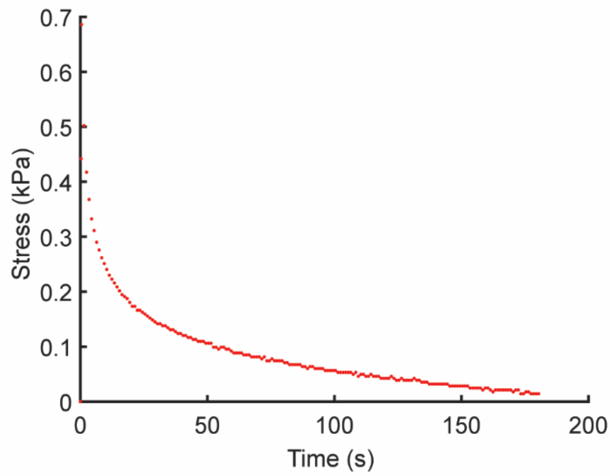

Figure S8| Stress relaxation curves of polyacrylamide gel. Indentation of polyacrylamide gel shows that the stress relaxation time is less than 4 minutes.

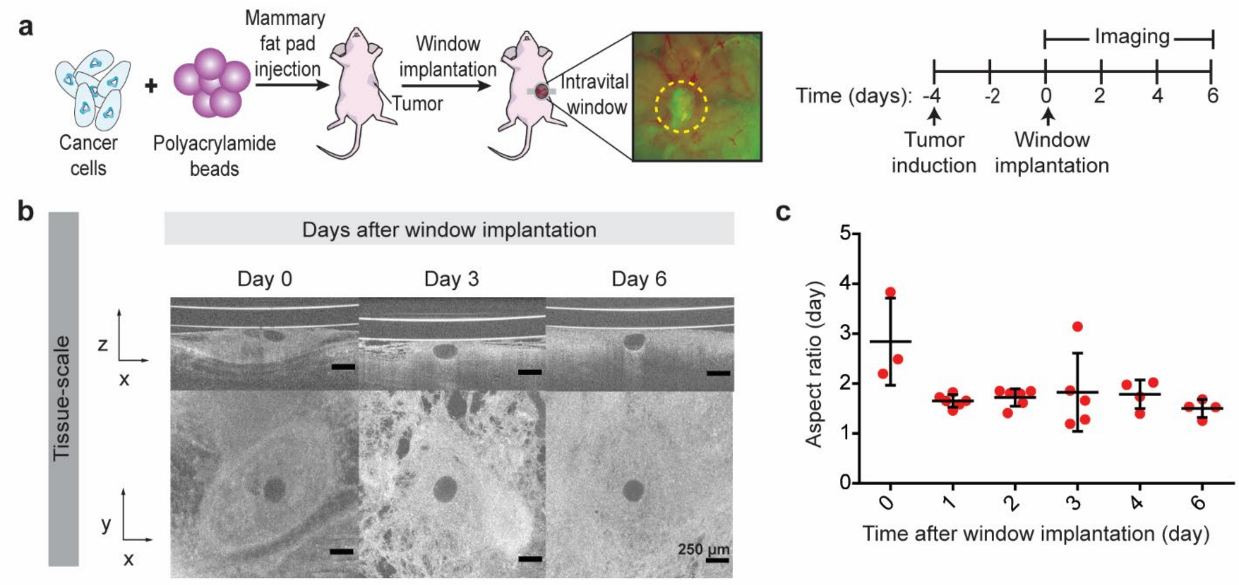

Figure S9| Window implantation after tumor growth causes artificial compression. a, Methodology and timeline for tumor induction. **b,** After demonstrating that window implantation after tumor formation applies artificial compression which relaxes over 6 days, we switched to window implantation before the tumor induction. We demonstrated that window implantation before the tumor induction does not alter the solid stress level (**Fig. 2h**). The XZ and XY views of bead in tumor at days 0, 3, and 6, captured with OCT. **c,** Aspect ratios of polyacrylamide beads over time (mean ± STD, n=3-6 beads).

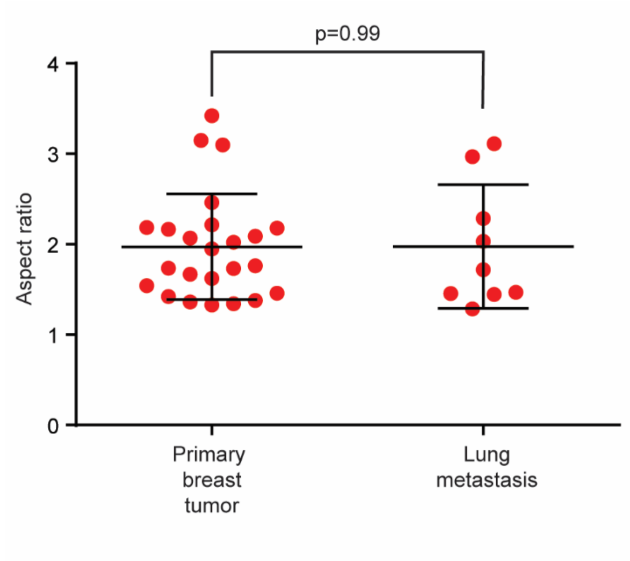

Figure S10| Comparison of PA microsphere aspect ratios in primary breast and micrometastatic lung cancer. Comparison of aspect ratio of polyacrylamide microsphere in primary MCa-M3C-H2B-dendra2 breast cancer and micrometastatic lung cancer. (mean ± STD, N=2-5 mice, n=9-33 microspheres, 2-sample t-test).

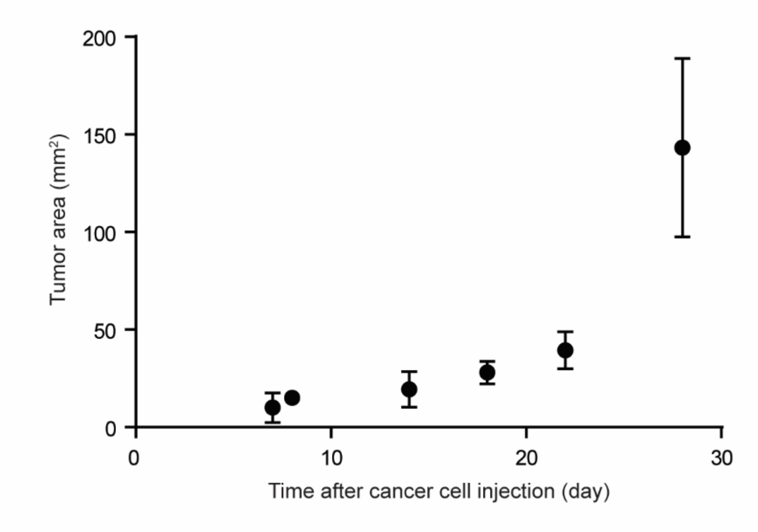

Figure S11| Tumor growth curve for the MCa-M3C-H2B-dendra2 cell line. Tumor area after MCa-M3C-H2B-dendra2 cancer cell injection under skin into mammary fat pad. (mean ± STD, N=5 mice)

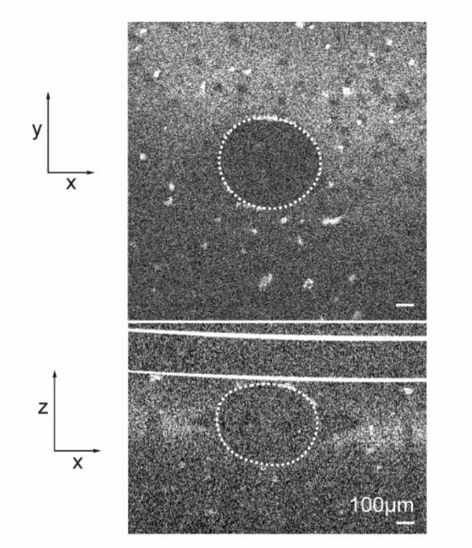

Figure S12| Embedding polyacrylamide beads and MCa-M3C-H2B-dendra2 cancer cells in Matrigel for day 0 imaging at tissue scale. Using polyacrylamide beads and MCa-M3C-H2B-dendra2 cancer cells embedded in Matrigel, beads can be visualized at the tissue-scale *in vivo* for longitudinal determination of solid stress from day 0

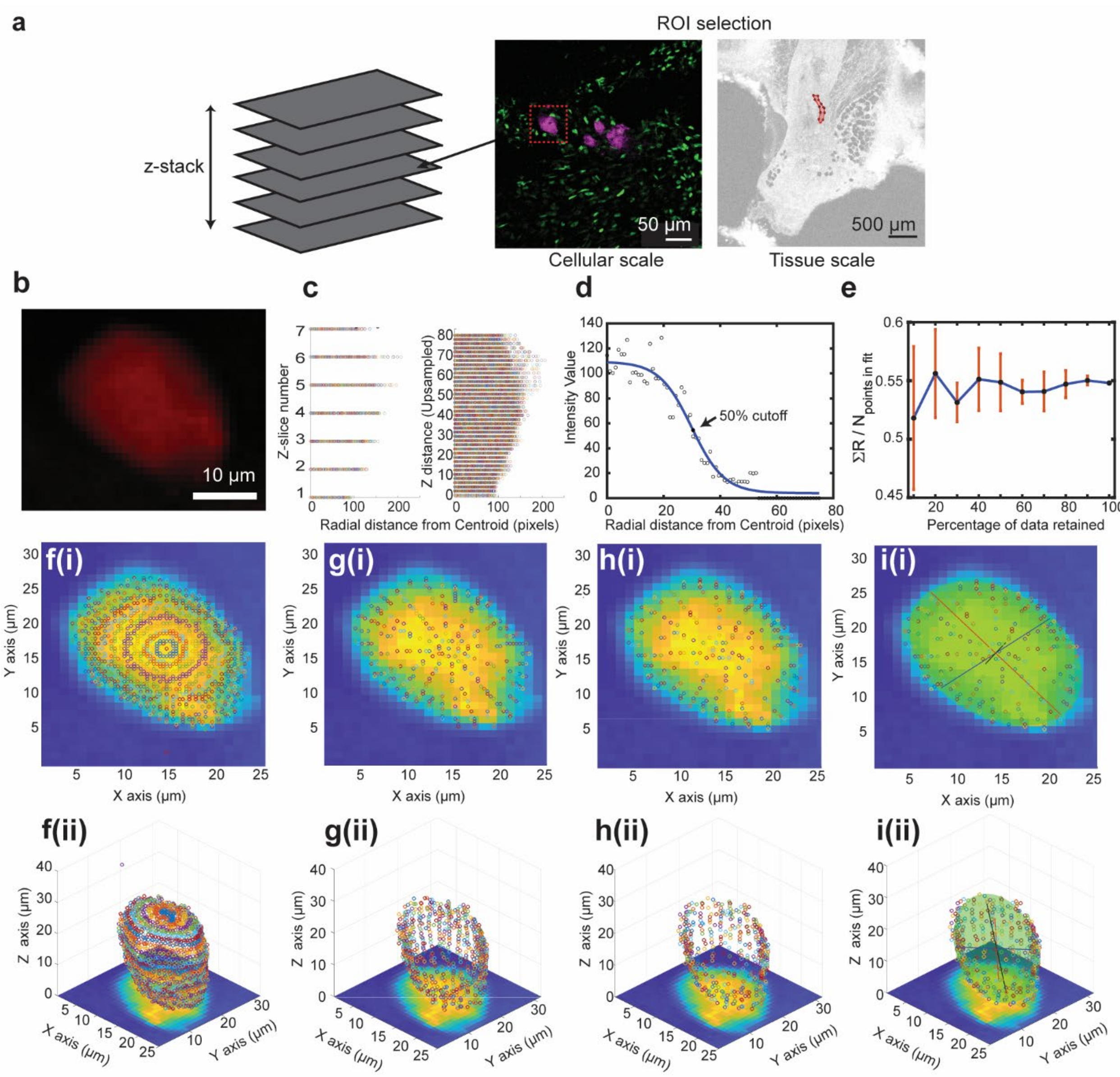

Figure S13| Image segmentation and ellipsoid fitting. a, ROI selection for cellular and tissue scales (cellular scale: beads (magenta), cancer cells (green), tissue scale: bead (outlined in red)). **b,** Bead of interest from a sample image. **c,** The image is up-sampled in the z-dimension to have a similar apparent resolution as in the x- and y-dimensions while preserving spatial information, as evident in the pixel projections along the radial distance from the centroid. **d,** From the centroid of the stack, radial paths are traced out through θ and ϕ values with gradual increments in ray length *r*. A sigmoid function is fit to the data and the 50% intensity value is taken to represent the boundary of the bead. **e,** After a reduction in data by θ and ϕ values, a final 60% of data is kept, as this value balanced a low residual distance between ellipsoid fit and data points (y-axis: sum of residuals normalized by number of points in the fit) and a reliable performance range (mean ± STD, n=10). **f-i (i),** Through the data down-sampling process the point cloud accurately captures the shape of the bead, as shown projected over the central plane. **f-i (ii)**, From the final ellipsoid fit, 3 principal axes lengths can be calculated.